Z. Phys. D 34, 171–184 (1995)

ZEITSCHRIFT
FÜR PHYSIK D

Population and deactivation of lowest lying barium levels by collisions with He, Ar, Xe and Ba ground state atoms

C. Vadla[1], K. Niemax[2], V. Horvatic[1], R. Beuc[1]

[1] Institute of Physics of the University, Bijenicka 46, 10000 Zagreb, Croatia
(Fax: + 385-1/421-156)
[2] Institut für Physik, Universität Hohenheim, Garbenstrasse 30, D-70599 Stuttgart, Germany
(Fax: + 49-711/459-2461)

Received: 14 February 1995 / Final version: 25 April 1995

Abstract. Excitation transfer between the barium low lying excited states $6s6p\ ^3P_1^0$, $6s5d\ ^1D_2$ and $6s5d\ ^3D_J$ by collisions with He, Ar, Xe and Ba has been investigated. The population densities in all levels involved were probed by absorption or by fluorescence using *cw* lasers. The depopulation cross sections of the Ba $^3P_1^0$ state by collisions with noble gases were found to be $\sigma_{He}(^3P_1^0) = 5.5 \cdot 10^{-16}\ cm^2$, $\sigma_{Ar}(^3P_1^0) = 4.6 \cdot 10^{-16}\ cm^2$, and $\sigma_{Xe}(^3P_1^0) = 1.7 \cdot 10^{-16}\ cm^2$. For Ar, the collisional depopulation of the $^3P_1^0$ level is exclusively due to the transition to the $^1D_2$ state. Under the assumption that the ^3D_J metastable states are populated collisionally by $^1D_2 \rightarrow {}^3D_J$ transfer only, we have deduced the upper limit for the corresponding cross section $\sigma_{13}^{Ar} = 1.5 \cdot 10^{-18}\ cm^2$. From the Ba $^1D_2$ and Ba ^3D_J steady-state diffusion distributions, collisional relaxation rates of the $^1D_2$ and ^3D_J levels were evaluated. The collisional relaxation rates by Ar and Ba yielded total cross sections for the depopulation of metastable levels: $\sigma_{Ar}(^1D_2) = 1.5 \cdot 10^{-17}\ cm^2$, $\sigma_{Ba}(^1D_2) \cong 1 \cdot 10^{-13}\ cm^2$, $\sigma_{Ar}(^3D_J) = 7 \cdot 10^{-21}\ cm^2$, and $\sigma_{Ba}(^3D_J) = 1 \cdot 10^{-15}\ cm^2$. Furthermore, it was found that the main contribution of the collisional depopulation of the $^1D_2$ state by Ar is related to back transfer to the $^3P_J^0$ state, whereas the deactivation of the ^3D_J metastable state is due to back transfer to the $^1D_2$ state. Taking into account other cross sections reported in literature we can conclude that collisional deactivation of both metastable levels by Ba ground state atoms can be attributed to their mutual collisional mixing.

PACS: 34.50; 32.00

1 Introduction

Recently we have studied energy pooling to high-lying levels of barium by pumping the low-lying $^3P_1^0$ level from the ground state in a noble gas atmosphere [1]. Energy pooling is the most important process to get an ion signal in laser enhanced ionization spectroscopy if low-lying states are excited. On the other hand, energy pooling processes generate non-linearities in the spectra [2, 3] which have to be taken into account in quantitative spectroscopy. For example, because of energy pooling the line intensities of the barium isotope components in the 791.3 nm line ($6s^2\ ^1S_0 \rightarrow 6s6p\ ^3P_1^0$ transition) were found to differ significantly from the true isotope ratio in the barium vapour [3]. Our recent investigation on the energy pooling in barium [1] gave hints that the populations of the high-lying levels depend also strongly on the populations of the Ba $6s5d\ ^3D_J$ and Ba $6s5d\ ^1D_2$ metastable levels which were populated by collisions and optical transitions. Furthermore, the metastable populations showed a strong dependence on the kind of the noble gas used in the cell and exhibited different spatial behaviour. In order to understand the experimental results of the energy pooling it was necessary to study the population and depopulation processes of these low-lying metastable levels.

The metastable $6s5d\ ^3D_J$ and $6s5d\ ^1D_2$ states are the first excited states in the barium term scheme (Fig. 1) and they are characterized by very long lifetimes. The radiative lifetime of the $6s5d\ ^1D_2$ level is about 0.2 *s* (0.125 *s* [4]; 0.24 *s* [5]), whereas the radiative lifetime of the $6s5d\ ^3D_J$ level is considerably longer (about 60 *s* [5]). The long radiative lifetimes of the $6s5d\ ^3D_J$ and $6s5d\ ^1D_2$ states arise from the fact that they are of the same parity as the $6s^2\ ^1S_0$ ground state. If barium atoms undergo collisions, collisional depopulation processes lower the lifetimes of metastable states. The metastable states can be populated by the excitation of higher-lying barium states and subsequent radiative and collisional relaxation. It has been shown earlier [6], that a very large fraction of all barium atoms can be found in the metastable levels if the $6s6p\ ^3P_1^0$ level is excited from the ground state by the intercombination transition at 791.3 nm. A direct consequence of large population densities in metastable states are pronounced energy pooling processes in barium.

In most experiments on excitation energy transfer in barium vapours, the atoms were excited from the ground state to the resonant $6s6p\ ^1P_1^0$ state by 553.5 nm laser

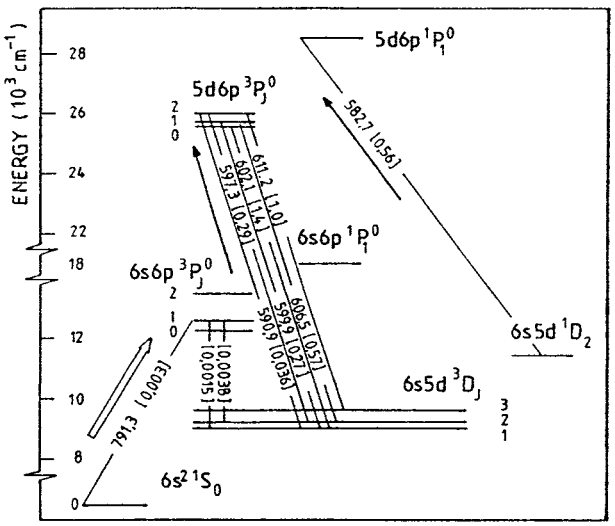

Fig. 1. Partial term diagram of barium with relevant optical transitions for which the wavelengths are given in nm. The *numbers in brackets* are the spontaneous transition probabilities in 10^8 s^{-1} taken from [13, 14]

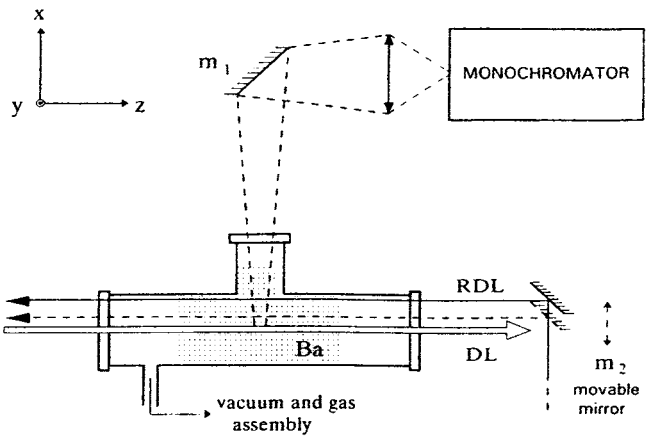

Fig. 2. Experimental arrangement; *RDL*, ring-dye laser beam; *DL* diode laser beam

radiation. The $^1P_1^0$ state is radiatively depopulated by transitions to the ground state and to the $^1D_2$ metastable state. As shown in [7, 8], an exclusive production of $6s6p\ ^3P_2^0$ occurs in collision between Ba($^1P_1^0$) and noble gas atoms. Collisional intermultiplet mixing for the ^3P_J states and the intramultiplet mixing processes involving ^3P_J, $^1D_2$ and ^3D_J were studied and several cross sections were obtained [9, 10] for transitions induced by collisions with both noble gas and ground state barium atoms.

Very recently, the depopulation of the Ba $6s5d\ ^3D_J$ and Ba $6s5d\ ^1D_2$ metastable levels by noble gas collisions has been studied using a tunable pulsed laser and time-resolved analysis [11]. In the present experiment, similar to [6], barium is excited to the $^3P_1^0$ level by 791.3 nm radiation. The measurements were performed in the steady state regime using tunable *cw* lasers for excitation. The population densities in all relevant levels involved have been probed by absorption or by fluorescence using *cw* lasers.

2 Experiment

2.1 Experimental arrangement

Figure 2 shows schematically the experimental arrangement used for the measurements of level populations in barium. A T-shaped stainless-steel cell filled with barium and one of the noble gases He, Ar or Xe was heated to temperatures of about 850 K. Barium ground-state atoms were optically excited to the $6s6p\ ^3P_1^0$ level by 791.3 nm radiation from a frequency stabilized, temperature and current-tuned single-mode diode laser (Hitachi HL7851, maximum power: 50 mW). The excitation process was controlled by monitoring the absorption through the metal vapour column (length $L = 4.5 \pm 1$ cm) of the $6s^2\ ^1S_0 \rightarrow 6s6p\ ^3P_1^0$ transition as well as by fluorescence of the 791.3 nm line from the interaction zone of the laser radiation with the metal vapour. The diode laser beam was expanded and collimated, and a circular aperture (diameter: 2 mm) cut the inner core. Therefore, behind the aperture the beam profile was nearly rectangularly shaped and the power was typically about 1.3 mW. In most measurements the radiation power had to be reduced by neutral density filters to values as low as about 5 μW. As already mentioned in the introduction, the metastable $6s5d\ ^3D_J$ and $6s5d\ ^1D_2$ levels are populated from the $6s6p\ ^3P_1^0$ level by radiative transitions as well as by collisions with noble gas atoms. The populations of the metastable triplet and singlet levels were measured by absorption of the $6s5d\ ^3D_J \rightarrow 5d6p\ ^3P_J^0$ and $6s5d\ ^1D_2 \rightarrow 5d6p\ ^1P_1^0$ transitions, respectively, applying a single-mode frequency-stabilized ring-dye laser (Spectra Physics 380D, dye: Rh6G). The counter propagating, collimated dye-laser beam, which will be called the probe beam, had a diameter of 1 mm. It was focused by a lens of long focal length (80 cm) to the centre of the cell. In that way, we obtained an uniform probe beam of Gaussian profile with a half-width of less than 0.5 mm in the vapour column. In order to avoid optical saturation, the power of the probe was kept low (less than 5 μW). The probe beam could be shifted parallel to the diode laser beam (Fig. 2). The absorption of both laser beams through the vapour column was detected by photodiodes.

The fluorescence of the relevant lines was measured by a 1 m McPherson monochromator (slit width: 500 μm) yielding a band width of about 0.5 nm. The fluorescence was imaged in 1:2 ratio onto the entrance slit of the monochromator. The radiation at the exit slit was measured by a RCA S20 photomultiplier.

Typical absorption and fluorescence spectra are shown in Fig. 3. In the upper spectra (Fig. 3a) the diode laser was scanned over the Ba $6s^2\ ^1S_0 \rightarrow 6s6p\ ^3P_1^0$ transition. Isotope structures can be seen (natural abundance: 71.7% ^{138}Ba, 11.2% ^{137}Ba, 7.9% ^{136}Ba, 6.6% ^{135}Ba, 2.4% ^{134}Ba). However, all measurements presented in this work were performed by locking the diode laser wavelength to the line centre of the main isotope ^{138}Ba and probing the populations of excited levels by scanning the dye laser.

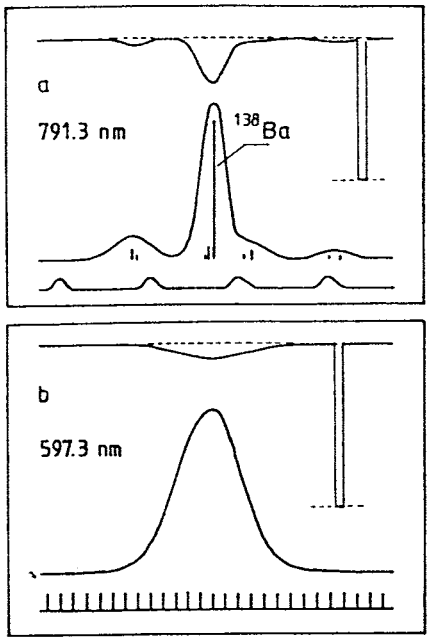

Fig. 3. a Simultaneously recorded absorption (*upper trace*) and fluorescence (*middle trace*) spectra of the barium 791.3 nm line. The spectra were obtained while the pump laser was scanned across the Ba $6s^2\,{}^1S_0 \rightarrow 6s6p\,{}^3P_1^0$ transition. Spectrum dispersion marks (*lower trace*) are separated by 2 GHz. **b** The spectra obtained in the case when the probe laser was scanned across the ^{138}Ba $6s5d\,{}^3D_2 \rightarrow 5d6p\,{}^3P_2^0$ transition while the diode laser was kept on the frequency corresponding to the centre of the ^{138}Ba $6s^2\,{}^1S_0 \rightarrow 6s6p\,{}^3P_1^0$ line. The dispersion marks are separated by 150 MHz

2.2 Method

The evaluation of the laser absorption and fluorescence data is based on the following considerations. The laser beam propagates in z-direction through the middle of the vapour column. Since the line width of the pump laser can be neglected compared with the width of the absorption line, the spectral intensity of the laser can be represented by:

$$J_0(\nu, \nu_l) = I_0\,\delta(\nu - \nu_l), \tag{1}$$

where I_0 and ν_l are the intensity and the frequency of the laser beam, respectively.

If the laser beam has passed a homogeneous vapour column of length z, the laser-light intensity $I_z(\nu_l)$ is given by:

$$I_z(\nu_l) = I_0 \exp[-k(\nu_l)\cdot z], \tag{2}$$

where $k(\nu_l)$ is the absorption coefficient.

If we denote the lower and the upper level of the transition by (1) and (2), respectively, the absorbed power $\Delta W_{1\rightarrow 2}$ in the region between z and $(z + \Delta z)$ is:

$$\Delta W_{1\rightarrow 2} = \Delta z\cdot s \int J_z(\nu, \nu_l) k_{12}(\nu)\,\mathrm{d}\nu$$

$$= \Delta z\cdot s\cdot k_{12}(\nu_l)\cdot I_0 \exp[-k_{12}(\nu_l)\cdot z], \tag{3}$$

where s is the cross section of the laser beam. The absorbed power will be spontaneously emitted from level 2. In general, in addition to the transition to level 1, there are several other branching transitions to the lower lying levels i. The fluorescence intensity $I_f^{2i} = N_2 A_{2i} h\nu_{2i}$ of a particular transition is proportional to the absorbed power, and it is emitted within the profile $P_{2i}(\nu)$ of the transition $2 \rightarrow i$. Therefore, the spectral intensity $J_f^{2i}(\nu)$ of the emitted fluorescence line is:

$$J_f^{2i}(\nu, \nu_l) \propto \Delta W_{1\rightarrow 2}\cdot P_{2i}(\nu). \tag{4}$$

The radiation from the fluorescence zone in the middle of the vapour column, at $z = L/2$, is observed at right angles in x-direction. The radiation passes the vapour layer of length d. Therefore, it is partially absorbed, i.e., it is attenuated by the factor $\exp[-k_{2i}(\nu)\,d]$. The fluorescence intensity detected by the broad-band monochromator is spectrally integrated over the frequencies within the $P_{2i}(\nu)$ profile:

$$I_{\mathrm{det}}^{2i}(\nu_l) \propto \Delta z\cdot s\cdot I_0\cdot k_{12}(\nu_l)\cdot \mathrm{e}^{[-k_{12}(\nu_l)\frac{L}{2}]}\cdot \int P_{2i}(\nu)\,\mathrm{e}^{-k_{2i}(\nu)\cdot d}\,\mathrm{d}\nu. \tag{5}$$

The absorption coefficient for the $1 \rightarrow 2$ transition is given by the well known expression [12]:

$$k_{12}(\nu) = N_1 \frac{g_2}{g_1}\frac{\lambda_{12}^2}{8\pi} A_{21} P_{12}(\nu), \tag{6}$$

where N_1 is the number density of the atoms in the lower state, g_1 and g_2 are the statistical weights of the lower and the upper state, respectively, and λ_{12} and A_{21} are the wavelength and the spontaneous emission coefficient of the transition under consideration, respectively.

The profiles of the barium lines measured in this work are generally of the Voigt type, i.e., the convolution of a Gaussian (Doppler broadening) and a Lorentzian function (pressure and natural broadening). The normalized Voigt profile is usually represented in the form:

$$P_{12}(\nu) = \frac{1}{\Delta\nu_D\sqrt{\pi}} H(\nu - \nu_{12}, a). \tag{7}$$

Here $H(\nu - \nu_{12}, a)$ is the Voigt function with the parameter $a = \Gamma_\nu/2\Delta\nu_D$, where Γ_ν is the Lorentzian half-width (FWHM, expressed in the units Hz) and $\Delta\nu_D = (\nu_0/c)(2kT/M)^{1/2}$ is Doppler constant.

The optical depths $k_{12}(\nu_l)\cdot L$ can be determined from the measured laser absorption spectra using (2), which yields:

$$k_{12}(\nu_l)\cdot L = -\ln\frac{I_L(\nu_l)}{I_0}. \tag{8}$$

With the known line profile one can easily determine the number density N_1 in the lower state from the measured peak absorption coefficients $k_{12}^0 = k_{12}(\nu_{12})$:

$$N_1 = k_{12}^0 \frac{g_1}{g_2}\frac{8\pi^{3/2}}{\lambda_{12}^3 A_{21}}\sqrt{\frac{2kT}{M}}\frac{1}{H(0,a)}. \tag{9}$$

The laser absorption method was used for lines with peak absorption depths $k_{12}^0 \cdot L$ in the range between 0.1 and 1.5. In the case of optically thin lines, i.e., for optical depths lower than 0.1, the fluorescence method was applied. For $k_{12}^0 \cdot L \ll 1$ the fluorescence signals are, according to (5), directly proportional to the corresponding absorption coefficient:

$$I_{\mathrm{det}}^{2i}(\nu_l) \propto \Delta z \cdot s \cdot I_0 \cdot k_{12}(\nu_l), \tag{10}$$

which yields the relative values for absorption coefficients and number densities N_1. The connection to the absolute scale was made by simultaneously measured absorption and fluorescence for $k_{12}^0 \cdot L$ values of about 0.1. This allows to calculate the absorption factor $\exp[-k_{12}(\nu_l) L/2] \cdot \int P_{2i}(\nu) \exp[-k_{2i}(\nu) \cdot d] \mathrm{d}\nu$ in (5) and to relate the obtained corrected fluorescence signals to the absolute values of the absorption coefficients.

In the evaluation of the results we used the values for spontaneous emission coefficients published in [13, 14].

3 Model

Because the lifetimes of the $6s5d\ ^3D_J$ and $6s5d\ ^1D_2$ states are long, their influence on the whole barium vapour system is significant. This will be described in the simplified case of a three level system, comprising the ground state (labelled with 1) and two excited states (labelled with 2 and 3). We assume that state 3, representing either Ba $^1D_2$ or Ba $^3D_1$, is metastable and below state 2, which in our case is level $6s6p\ ^3P_1^0$. The depopulation processes $2 \to 1$, $2 \to 3$ and $3 \to 1$ are described by relaxation rates A_{21}, A_{23} and A_{31}, respectively. In the case when state 2 is optically excited with the pumping rate $\rho_0 B_{12}$, ρ_0 being the spectral density of the incident radiation and B_{12} the Einstein coefficient for the absorption process $1 \to 2$, the steady state rate equations for the population densities N_3 and N_2 are:

$$\frac{\mathrm{d}}{\mathrm{d}t} N_3 = 0 = N_2 A_{23} - N_3 A_{31}, \tag{11}$$

$$\frac{\mathrm{d}}{\mathrm{d}t} N_2 = 0 = \rho_0 B_{12} N_1 - N_2 (A_{21} + A_{23}). \tag{12}$$

If we denote the total number density of the atoms by $N_0 = N_1 + N_2 + N_3$, the above equations yield the number density N_1 of the ground-state atoms:

$$N_1 = \frac{N_0}{1 + \dfrac{\rho_0 B_{12}}{A_{21} + A_{23}} \left(1 + \dfrac{A_{23}}{A_{31}}\right)}. \tag{13}$$

Since the level 3 is assumed to be metastable, its relaxation rate A_{31} is small compared with other rates considered. Therefore, the ratio A_{23}/A_{31} is much larger than 1. In that case, (13) shows that even for excitation far from optical saturation ($\rho_0 B_{12} \ll A_{21} + A_{23}$) saturation-like effects can be expected because the factor A_{23}/A_{31} can substantially dominate the second term in the denominator. Thus, the ground state is depleted at the expense of the population of the metastable state. For example, our laser beam of 2 mm diameter and 100 μW power produced a ground state depletion of about 20%. The corresponding optical pumping rate can be estimated from the relation between the Einstein coefficient and the classical absorption coefficient:

$$\rho_0 B_{12} = \frac{1}{8\pi^{3/2}} \frac{\lambda_{12}^3 A_{21}}{hc \Delta\nu_D} \frac{g_2}{g_1} \frac{q}{s}, \tag{14}$$

which is valid for the centre of the Doppler broadened line. Here, q and s are the power and the cross section of the laser beam, respectively. In our example, the pump rate of the $^1S_0 \to {}^3P_1^0$ transition was $\rho_0 B_{12} = 4 \cdot 10^3\ \mathrm{s}^{-1}$. This is small compared with the spontaneous emission relaxation rate $(A_{21} + A_{23}) = 8.3 \cdot 10^5\ \mathrm{s}^{-1}$ [13]. Therefore, the optical saturation is negligible. The ground state depletion is due to the large population to depopulation ratio A_{23}/A_{31}, being about 40 in our case.

Furthermore, when the radiation has passed the vapour column by z, its intensity is attenuated by the $1 \to 2$ absorption process. The ground-state number density N_1 is dependent on position z, and, consequently, (13) can be rewritten in the form:

$$N_1(z) = \frac{N_0}{1 + \beta \cdot \exp[-b \cdot N_1(z) \cdot z]}, \tag{15}$$

where the factor β is identical with the second term in the denominator of (13) while b can be easily derived from (6).

In our consideration, the relaxation rates of the excited states have been assumed to be much greater than the diffusion rates, leaving excited atoms confined only in the laser beam volume. In the next step, we consider that the latter assumption is valid only for the state 2, while the relaxation rate A_{31} is comparable with the diffusion rates. In this case, for a laser beam of radius r_0 and constant spatial power density, the atoms in state 2 have the simple spatial distribution:

$$N_2(r) = N_2 \sigma(r, r_0), \tag{16}$$

where the function $\sigma(r, r_0)$ equals 1 for $r \leq r_0$ and 0 for $r > r_0$. The atoms in the state 2 represent the population source for creation of the atoms in state 3 which diffuse out of the laser excitation region. By inclusion of the diffusion term, the rate equation (11) becomes a steady-state diffusion equation for N_3:

$$D \nabla^2 N_3(r) - N_3(r) A_{31} + S(r, r_0) = 0. \tag{17}$$

Here, $S(r, r_0) = N_2 A_{23} \sigma(r, r_0)$ is the source function for the population of state 3 and D is the diffusion coefficient which is, according to the kinetic theory of gases, given as function of pressure p and temperature T via:

$$D = D_0 \frac{p_0}{p} \left(\frac{T}{T_0}\right)^{3/2}, \tag{18}$$

where D_0 is the diffusion constant for the particular diffusion process at $p_0 = 1$ atm and $T_0 = 273$ K.

The metastable atoms diffuse from the excitation zone and their steady state distribution, depending on geometry and physical conditions, produces a corresponding

radial distribution of atoms in other states. Outside the laser excitation volume, the density of the atoms in the metastable state 3 obeys the Bessel's modified differential equation of zero order which, with the substitution $\xi = \sqrt{A_{31}/D} \cdot r$, can be written in the form:

$$\left[\frac{\partial^2}{\partial \xi^2} + \frac{1}{\xi}\frac{\partial}{\partial \xi}\right] N_3(\xi) - N_3(\xi) = 0. \tag{19}$$

The solution of the above equation damps exponentially with distance r for $\xi \gg 1$ and this condition can be useful for rough comparison between the relaxation and diffusion rates. For instance, the atoms in state 3 will be primarily confined within the laser beam of radius r_0, if $A_{31} \gg D/r_0^2$.

The relaxation rates can generally be represented as the sum of the spontaneous relaxation rate A_0 and collisional contributions:

$$A = A_0 + \sum_i N_i v_i \sigma_i. \tag{20}$$

Here N_i is the number density of the i-th colliding partner, v_i is the mean relative velocity and σ_i is the corresponding cross section for particular collisional processes (quenching, mixing of the populations, etc.).

The optically excited barium vapours behave in many details as the model described. The incident laser radiation transfers the ground state atoms via relaxation of the higher states to the low-lying metastable states which diffuse out of the excitation zone. As shown later in this work (Sect. 4.6 and 4.7), the barium metastable levels are characterized by very small A_0 values and, at the given experimental conditions, their actual relaxation rates are essentially determined by collisional deactivation processes. Due to this fact, the spatial distributions of the metastable barium atoms in optically excited barium vapours depend not only on the geometry of the experiment but also on the given experimental parameters, making this system very complex.

4 Results

4.1 Depletion of the barium ground state and the barium number density

The optical depth $k^0_{791.3} \cdot L$ at the centre of the Ba 791.3 nm line was measured in dependence on buffer gas pressure as well as on laser power. The barium number density was chosen to be in the range where $^3P_1^0 \rightarrow {}^1S_0$ radiation exhibits no trapping effects. Therefore, the number density of barium $^3P_1^0$ atoms is homogeneous within the laser beam. The results are shown in Fig. 4 for argon as a buffer gas. Qualitatively, the same behaviour was obtained for He and Xe. According to [15], the noble gas pressure broadening constants γ_ω (in angular frequencies) of the 791·3 nm line are of the order of $3 \cdot 10^{-9}$ cm^3 rad s^{-1}. The noble gas number density N_p was varied between $3 \cdot 10^{15}$ cm^{-3} and $5 \cdot 10^{16}$ cm^{-3}, corresponding to

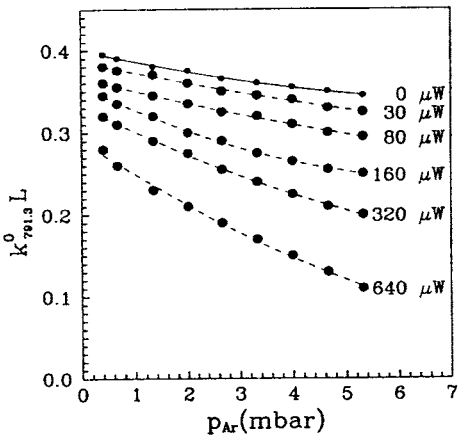

Fig. 4. The peak absorption coefficient of the 791.3 nm line vs. argon pressure in dependence on the laser beam power. The *full line* represents the extrapolation to zero power. The *numbers* associated with each curve are the applied powers in μW

pressures between 0.3 and 5 mbar at $T \approx 830$ K. This gives maximum Lorentzian widths $\Gamma_\nu = \gamma_\nu N_p$ of about 25 MHz, which is more than one order of magnitude smaller than the Doppler constant ($\Delta\nu_D = 400$ MHz). Consequently the minimal value of $H(0, a)$ is about 0.98, which means that the shape of the line core can be regarded as almost a pure Doppler profile. The barium ground-state number density is related to the measured peak optical depths via (9) and can be calculated by putting $H(0, a) = 1$, which is valid in the case of a Doppler profile.

In Fig. 4 one can see that a significant depletion of the barium ground state atoms (about 80%) can be produced by relatively weak laser intensities in the noble gas pressure range applied. Note, that even the curve obtained by extrapolation to zero power shows a slow decrease with increasing buffer gas pressure. However, this slow decrease is not associated with the depletion of the ground state due to collisional transfer to metastable levels, but is caused either by a change of the Ba ground state density $N(^1S_0)$ or by a change of the vapour column length L, because collisional effects (up to 5 mbar) are negligible as shown above ($H(0, a) \approx 0.98$). It is not possible to distinguish between them because the measurements are related to the product $N(^1S_0) \cdot L$. In comparison with argon, the depletion of the barium ground state is stronger for helium and weaker for xenon.

We have determined the barium atom number densities from the absorption of the 791.3 nm line. In order to avoid the depletion of the ground state, a weak (5 μW) laser beam was used. The temperature of the Ba vapour was evaluated from the wing of the Doppler broadened 611.2 nm line with an accuracy of ± 15 K. The profile of this line was measured in fluorescence by probing the $^3D_3$ level. The measurements were performed in Ar at gas pressures between 0.5 and 1 mbar. The results are shown in Fig. 5. In comparison with the results obtained in a similar arrangement [15], this curve lies somewhat higher. However, there is still an overlap of the mutual error bars. In comparison with the data from the vapour pressure curves of [16], our values are lower by a factor of 6.

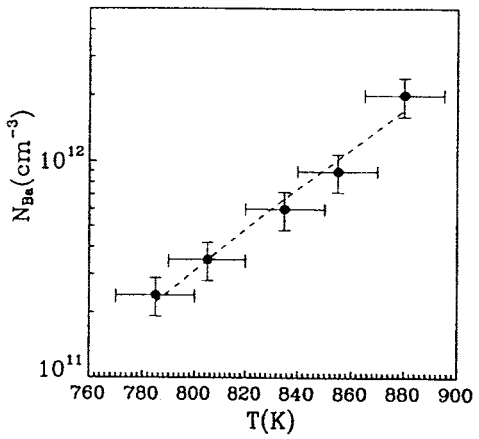

Fig. 5. The number density of the barium atoms as a function of temperature. The *error bars* are determined by the accuracy with which the vapour column length (± 20%) and temperature (± 15 K) are known

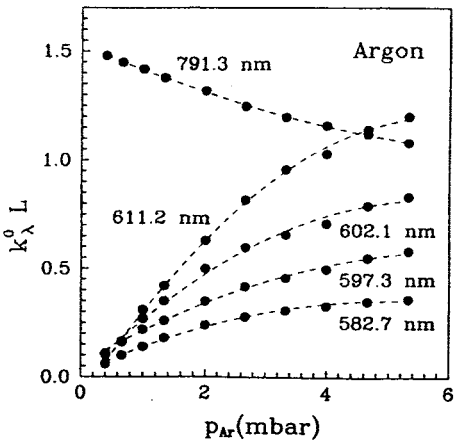

Fig. 6. The optical depths of 582.7 nm, 602.1 nm, 597.3 nm, and 611.2 nm barium lines relevant for determination of $^1D_2$, $^3D_1$, $^3D_2$, and $^3D_3$ populations, respectively, together with optical depth of the 791.3 nm, line shown as a function of argon pressure (for particular experimental conditions given in Sect. 4.3)

4.2 Collisional populations of the barium ^3D_J and $^1D_2$ states

The optical depths $k_\lambda^0 \cdot L$ of the 611.2 nm, 597.3 nm, 602.1 nm and 582.7 nm lines, which give information on the populations of the $^3D_3$, $^3D_2$, $^3D_1$ and $^1D_2$ levels, respectively, were measured as a function of both noble gas pressure and pump laser power. The collinear probe beam was aligned to the axis of the pump beam. Therefore, the experimental data corresponded to the centre of the excitation volume. For a constant pressure, the optical depths of the absorption lines from metastable levels increased with pump power. Below a noble gas pressure of about 1.5 mbar the dependence was nearly linear in the power range 100–1000 μW.

Figure 6 shows results of absorption measurements with argon as a buffer gas. The pump laser was locked to the centre of the 791.3 nm line. The power of the pump laser was 400 μW producing significant depletion of the ground-state number density. This depletion was monitored by simultaneous measurement of the peak absorption of the 791.3 nm line. Under the same conditions, the measurements were performed also with Xe and He. From the absorption data the corresponding densities $N(^1S_0)$, $N(^3D_J)$ and $N(^1D_2)$, which are average densities along the probe beam, were calculated. All lines had Doppler profiles in the cores for the noble gas pressures applied. Therefore, the number densities could be calculated using (9) with $H(0, a) = 1$.

The relative populations of the ^3D_J sublevels, $N(^3D_3)/N(^3D_1)$ and $N(^3D_2)/N(^3D_1)$, are shown in dependence on argon pressure in Fig. 7. Similar curves have been obtained for helium and xenon. In the zero pressure limit, $N(^3D_3)/N(^3D_1)$ converges to zero whereas $N(^3D_2)/N(^3D_1)$ approaches the value 2 which is expected from the branching ratio of the spontaneous emission transitions $^3P_1^0 \rightarrow {}^3D_J$. For pressures larger than 2 mbar, $N(^3D_3)/N(^3D_1)$ and $N(^3D_2)/N(^3D_1)$ are in good agreement with the predicted ratios from thermodynamic equilibrium, which are 1.2 : 1 and 0.82 : 1, respectively. This means

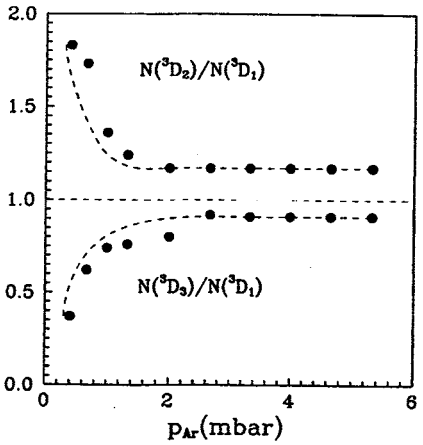

Fig. 7. Relative populations of the ^3D_J sublevels against noble gas pressure, obtained from the data plotted in Fig. 6. The curves exhibit complete intramultiplet mixing for pressures above 2 mbar

that intermultiplet mixing is complete at 2 mbar. The pressure dependent ratio of the total number density of the metastable triplet states $N(^3D_J)$ and the number density of the depleted ground state $N(^1S_0)$ is displayed in Fig. 8. The ratios $N(^3D_J)/N(^1S_0)$ are very similar for argon and helium, whereas the ratios are about a factor of 2 larger for xenon than for other noble gases investigated. The pressure dependent ratios of the number densities of the singlet and triplet metastables show very different behaviour which depend on the kind of buffer gas (Fig. 9). It has to be emphasized that the ratios $N(^1D_2)/N(^3D_J)$ do not show any dependence on the power of the pump laser, while in contrast, the ratios $N(^3D_J)/N(^1S_0)$ do show strong dependence on the laser power.

Taking into account the experimental temperatures, the ratio $N(^1D_2)/N(^3D_J)$ in thermal equilibrium is predicted to be about 0.01. In Fig. 9 can be seen that this ratio is about 0.3 for argon at low pressures and decreases slowly with increasing pressure. This indicates a very poor

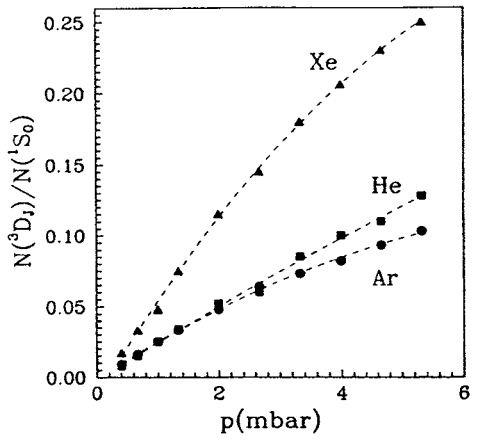

Fig. 8. The ratio of the total triplet to ground-state barium number density in dependence on He, Ar and Xe pressure. The measurements shown were performed using 400 μW pump laser power. The results are obtained from the data given in Fig. 6

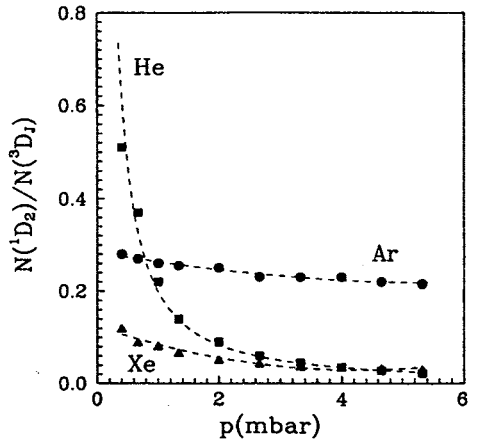

Fig. 9. The ratio of the singlet to triplet metastable number densities as a function of He, Ar and Xe pressure. The number densities were measured on the axis of the pump laser beam

coupling between the $^1D_2$ and ^3D_J states. In the case of He, the $N(^1D_2)/N(^3D_J)$ ratio is higher than in argon at low pressures and decreases sharply, reaching the equilibrium value for $p > 4$ mbar. This indicates a strong collisional mixing between the metastable states. The low pressure values $N(^1D_2)/N(^3D_J)$ for Xe are lower than for Ar and He. However, in terms of $^1D_2$ and ^3D_J mixing, xenon represents an intermediate case.

4.3 Depopulation rates of the barium $^3P_1^0$ atoms due to collisions with He, Ar and Xe

From the results presented in the previous section, it can be concluded that the metastable barium $^1D_2$ and ^3D_J levels are primarily populated by collisions of Ba($^3P_1^0$) and noble gas atoms (Fig. 6). In order to determine the ratio of collisional to radiative depopulation of the $^3P_1^0$ level, the variation of the number density $N(^3P_1^0)$ in dependence on noble gas pressure was measured by fluorescence of the 791.3 nm intercombination line.

If we denote the total collisional depopulation rate by R, the simple steady-state rate equation for the $^3P_1^0$ level, in which the contributions by collisional repopulation are neglected, is given by:

$$N(^3P_1^0) = \frac{\rho B}{A_{21} + A_{23} + R} N(^1S_0). \tag{21}$$

Here, ρB is the pump rate of the $^1S_0 \rightarrow {}^3P_1^0$ transition, while A_{21} and A_{23} are the spontaneous emission rates for $^3P_1^0 \rightarrow {}^1S_0$ and $^3P_1^0 \rightarrow {}^3D_J$ transitions, respectively.

The fluorescence intensity I_f of the $^3P_1^0 \rightarrow {}^1S_0$ line emitted from an optically thin layer is proportional to the product $N(^3P_1^0) \cdot A_{21}$ and, in accordance with (21), its dependence on noble gas density is given by:

$$I_f(N_p) \propto \rho B \frac{A_{21}}{A_{21} + A_{23} + N_p v \sigma} N(^1S_0), \tag{22}$$

where N_p is the perturber number density. If the fluorescence intensity is normalized to the signal at zero perturber number density we obtain with (22):

$$I_N(N_p) = \frac{I_f(N_p)}{I_f(0)} = \frac{A}{A + N_p v \sigma}, \tag{23}$$

where $A = A_{21} + A_{23}$.

The expression (23) was used for the determination of the depopulation cross section of the $^3P_1^0$ level. The fluorescence intensity as well as the optical depth of the 791.3 nm line were measured for noble gas pressures from 4 mbar to 0.1 mbar. In order to minimize the depletion of the ground state, the measurements were performed with low laser power (about 10 μW). The detected peak fluorescence signals of the ^{138}Ba 791.3 nm line were corrected for the absorption factor (Eq. 5) which was calculated using the measured optical depth of the line. The corrected fluorescence intensities were normalized to zero noble gas pressure. As shown in Sect. 4.1, the optical depth $k^0_{791.3} \cdot L$ slightly varies with noble gas pressure. On the other hand, the fluorescence intensities are proportional to $k^0_{791.3}$. If the change of the optical depth is only due to the change of L, the intensities have to be corrected only for the absorption factor, i.e., the measured relative intensities have to be divided by the factor $\exp[-kL/2] \cdot \int P(v) \exp[-k(v) \cdot d] dv$. In the case when the change of $k^0_{791.3} \cdot L$ is caused by variation of the ground state atom number density, the measured intensities have to be divided additionally by $k^0_{791.3}$ before normalization. The normalized intensities obtained by applying the first and the second procedure are labelled with I'_N and I''_N, respectively, representing the minimum and maximum intensities possible. For example, the results obtained for xenon are displayed in Fig. 10.

The values $\eta = (1 - I_N)/I_N$, evaluated from the measurements in He, Ar and Xe and plotted against the noble gas pressure, are shown in Fig. 11. Using these data, one can obtain the cross sections which, according to (23), are given by:

$$\sigma = \frac{A}{N_p \cdot v} \eta. \tag{24}$$

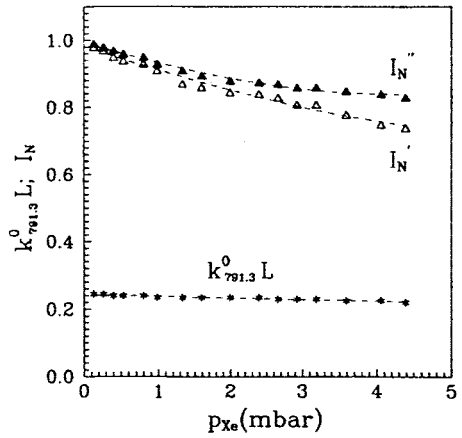

Fig. 10. The normalized intensities of the Ba 791.3 nm line versus Xe pressure. I_N' and I_N'' represent the lowest and the highest intensities possible. Further explanations are given in Sect. 4.3

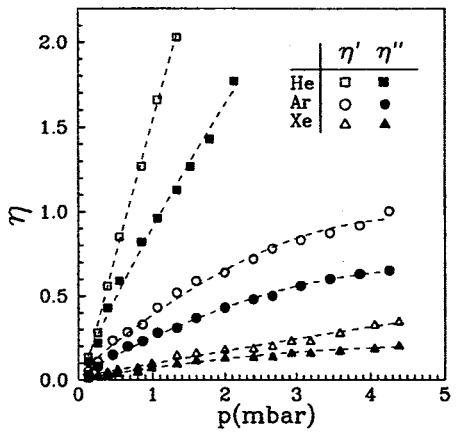

Fig. 11. The values $\eta = (I - I_N)/I_N$ in dependence on Xe pressure (see Sect. 4.3 for further explanations)

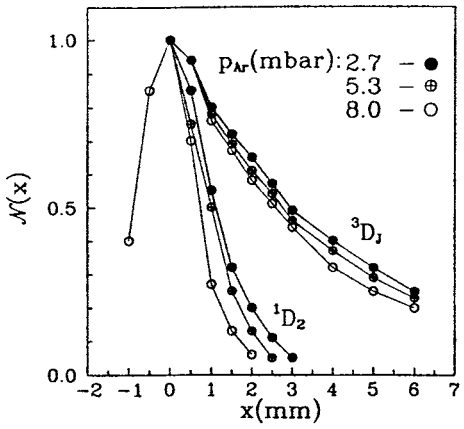

Fig. 12. The spatial distributions of Ba $^1D_2$ and Ba ^3D_J metastable atoms in argon

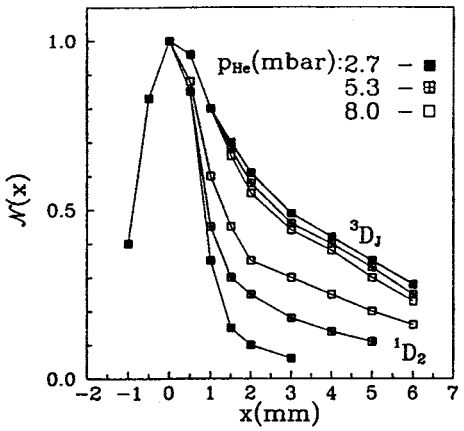

Fig. 13. The spatial distributions of Ba $^1D_2$ and Ba ^3D_J metastable atoms in helium

In the evaluation, η values measured at low pressures were used. This is very important, since η showed strong deviations from linearity for higher pressures (Fig. 11) and, therefore, the simple rate equation (21), in which the collisional repopulation of the $^3P_1^0$ state is neglected, is no longer valid.

Taking into account the total radiative relaxation rate $A = 8.3 \cdot 10^5\ s^{-1}$ [13], the following collisional depopulation cross sections were found at the experimental temperature $T = 760$ K:

$$\sigma_{He}(^3P_1^0) = 5.5 \cdot 10^{-16}\ cm^2 \quad (25)$$

$$\sigma_{Ar}(^3P_1^0) = 4.6 \cdot 10^{-16}\ cm^2 \quad (26)$$

$$\sigma_{Xe}(^3P_1^0) = 1.7 \cdot 10^{-16}\ cm^2. \quad (27)$$

The estimated error bar of our results is about $\pm$ 30%. It is mainly due to the uncertainty in the absorption coefficient of the 791.3 nm line.

The collisional depopulation rates for the $^3P_1^0$ levels include, in general, the rates for collisional intramultiplet mixing $^3P_1^0 \rightarrow {}^3P_0^0, {}^3P_2^0$ and the intermultiplet transitions $^3P_1^0 \rightarrow {}^1D_2, {}^3D_J$. According to [9] the cross sections $\sigma(^3P_1^0 \rightarrow {}^3P_0^0)$ and $\sigma(^3P_1^0 \rightarrow {}^3P_2^0)$ for the collisions with noble gas atoms are negligible in comparison with the total depopulation cross sections obtained in our experiment. For example, in [9] the following data for argon were reported: $\sigma(^3P_1^0 \rightarrow {}^3P_0^0) = 6 \cdot 10^{-19}\ cm^2$ and $\sigma(^3P_2^0 \rightarrow {}^3P_1^0) = 1.2 \cdot 10^{-18}\ cm^2$. Therefore, it can be concluded that the depopulation cross sections measured in the present experiment are related only to the collision induced transitions $^3P_1^0 \rightarrow {}^1D_2$ and $^3P_1^0 \rightarrow {}^3D_J$.

4.4 The diffusion of the barium ^3D_J and $^1D_2$ atoms

The spatial distributions of metastable barium atoms in and outside the region of the laser beam were measured by fluorescence. The probe laser beam was tuned to the centres of the optically thin lines 590.9 nm, 597.3 nm and 611.2 nm for the measurement of the ^3D_J distribution, or to the centre of the 582.7 nm line, for the $^1D_2$ distribution. The probe beam was shifted up to 6 mm from the axis of the pump beam. A 4 mm long part of the probe beam was imaged parallel to the slit (height 2 mm, width 500 μm) onto the monochromator. The translation of the

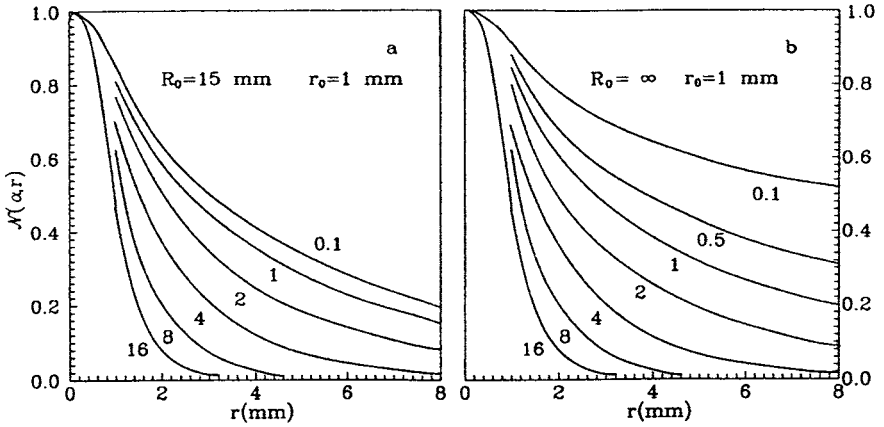

Fig. 14a, b. The calculated spatial distributions for metastable barium atoms. The parameters α (numbers associated with each curve) are given in cm^{-1}. **a** The curves obtained if recombination on the cell walls is assumed, i.e., solutions of the diffusion equation for boundary condition $(\alpha, R_0) = 0$, where R_0 is the radius of the cell. **b** The solutions for the case of infinite cell radius R_0

fluorescence zone was compensated by readjustment of the imaging lens. The detected fluorescence intensities $I(x)$, which are proportional to the corresponding metastable atom number densities, were normalized to the intensities $I(0)$ at the central position ($x = r = 0$), yielding the relative distribution $\aleph(x) = I(x)/I(0)$ of the particular metastable atom number density.

The results of the measurements in argon and helium are plotted in Figs. 12 and 13, respectively. The spatial distributions of Ba ^3D_J metastable atoms are similar for both noble gases in the pressure range 2.7 – 8 mbar. The results for Xe, which are not shown, are comparable with He and Ar in that pressure region. However, due to the different diffusion of barium atoms in He, Ar and Xe, there are differences in the distributions for pressures larger than 8 mbar. According to [17] the D_0 data for diffusion of Ba ^3D_J in He, Ar and Xe, are $0.56\,cm^2\,s^{-1}$, $0.143\,cm^2\,s^{-1}$ and $0.084\,cm^2\,s^{-1}$, respectively. On the other hand, the distribution curves of Ba ^3D_J atoms become wider with decreasing pressure and reach the widest shape at about 2.7 mbar. Below 2.7 mbar, the distribution profiles gently narrow again. This finding implies that the recombination on the cell walls is the main relaxation mechanism of the Ba ^3D_J metastables in the pressure range below 8 mbar.

In the case of Ba $^1D_2$, the atoms are more confined within the laser beam volume. This indicates a faster relaxation than for Ba ^3D_J. The spatial distribution of the singlet atoms in argon exhibits the expected behaviour, i.e., the lower the pressure the more pronounced is the diffusion. The measured diffusion curves for Ba $^1D_2$ in Ar fit very well into the field of theoretical curves computed for the geometry present in this experiment (see next section). In the case of He, the distribution of Ba $^1D_2$ atoms shows a pressure dependence which is opposite to the theoretical expectation: with increasing pressure the distribution curves are getting wider. On the other hand, the slopes of these curves deviate strongly from the calculated diffusion distributions. Obviously, the distribution of the Ba $^1D_2$ metastables in He is not primarily governed by the diffusion process but by other mechanisms. The distribution shapes of ^3D_J and $^1D_2$ atoms in He suggest, unlike in Ar, that there is a strong collisional mixing between these states due to collisions with noble gas atoms.

Collisional mixing between barium in $^1D_2$ and ^3D_J states has also to be assumed in Xe. However, the influence on the distribution is weaker than in helium.

4.5 Comparison between experimental and theoretical diffusion curves

As can be seen in Fig. 9, there is very weak collisional mixing of the Ba $^1D_2$ and ^3D_J metastable levels in argon. This was investigated for Ar pressures up to 30 mbar. At the pressure of 30 mbar the ratio $N(^1D_2)/N(^3D_J)$ was about 0.033, which is still three times larger than the ratio expected in thermal equilibrium. It means that the diffusion of singlet and triplet metastable barium atoms in argon can be considered as independent processes. Consequently, in the steady-state diffusion equations for singlet and triplet barium number densities, the terms involving coupling between them can be neglected. Thus, the diffusion in each case can be described by a separate equation. For the given boundary conditions, the solutions of the steady-state diffusion equation are characterized by the parameter $\alpha = \sqrt{A/D}$. The parameter can be determined from experiment by a fit of the measured diffusion distribution to the theoretical curves. With known diffusion coefficient D, the relaxation rate A of the diffusing metastable atoms can be determined.

For the evaluation of the relaxation rates $A(^1D_2)$ and $A(^3D_J)$ of the barium metastable levels, the theoretical diffusion curves were calculated from (17). A rectangular source function $\sigma(r, r_0)$ with $r_0 = 0.1$ cm was applied. This function is very close to the shape of the laser beam in the experiment. The assumption was made that there is complete recombination of the metastables at the cell walls. Therefore, the metastable number density is zero at $r = R_0 = 1.5$ cm, the radius of the cell. The calculated curves (α, r) normalized to $(\alpha, 0)$ are plotted in Fig. 14a. In order to check the influence of the cell walls we calculated the solutions of the diffusion equation for $R_0 = \infty$. The results are given in Fig. 14b. It can be seen in Figs. 14a and b, that the calculated curves in both cases show no difference for $\alpha > 8\,cm^{-1}$. However, there is an obvious difference between the curves obtained for finite and infinite geometry for lower values of α. The curves for the

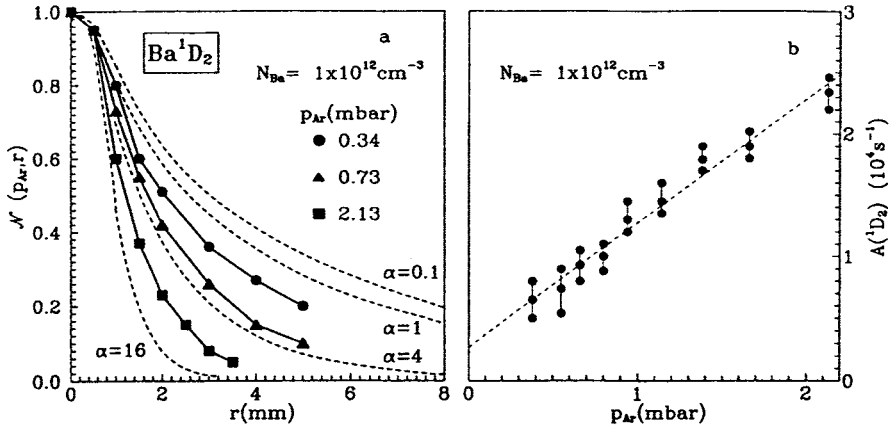

Fig. 15. **a** The measured and calculated distributions for Ba $^1D_2$ diffusion in argon. The measurements were performed at constant Ba ground state number density. **b** The relaxation rates of the $^1D_2$ level, deduced from the data in part **a** of this figure, plotted against argon pressure. For particular pressures the evaluation took into account the data at r = 3, 4, 5 cm

experimental geometry (R_0 = 1.5 cm) converge in the same way as the experimental curves for ^3D_J metastables do (see Figs. 12 and 13). This confirms the validity of the assumed boundary condition (α, R_0) = 0.

The experimental diffusion curves were obtained with laser pump powers between 10 and 100 μW. For each measurement the pump power was optimized in order to minimize the depletion of the ground state, and, on the other hand, to provide measurable intensities of the fluorescence lines used for probing the metastable number densities.

As can be seen in Fig. 14a, the calculated diffusion distributions show the biggest difference with respect to relative changes of α for parameter α between 1 cm^{-1} and 10 cm^{-1}. The experimental diffusion curves have error bars of about 0.5 mm for r and 10% for (α, r). Therefore, the fitting to the calculated curves with α outside the mentioned region produces too large uncertainties in α. For that reason, the diffusion rates of the Ba metastables should be appropriately adjusted with respect to their relaxation rates, in order to give the experimental diffusion curves in the required region. In the case of Ba $^1D_2$ metastables this was achieved at argon pressures of the order of magnitude 1 mbar. For the Ba ^3D_J metastables, which have significantly smaller relaxation rates, a correspondingly smaller diffusion coefficient was required, so that the measurements were performed at Ar pressures one order of magnitude higher than in the experiment on the Ba $^1D_2$ atoms.

4.6 Relaxation of the barium $^1D_2$ atoms

The number density of barium $^3P_1^0$ atoms was homogeneously distributed within the cylindrical volume of the laser beam. Since in the case of argon as a buffer gas, the $^3P_1^0$ level is the only possible source for creation of $^1D_2$ metastables, the assumption of a rectangular shape of the source function $\vartheta(r, r_0)$ is valid for the Ba $^1D_2$ diffusion process.

For example, we have displayed three experimental diffusion distributions together with several theoretical curves in the Fig. 15a. The measured distribution curves fit very well into the field of the calculated curves. The measurements were performed in the Ar pressure range between 0.3 and 2.2 mbar. The diffusion distributions obtained correspond to theoretical curves with parameters α in the range from 1.8 cm^{-1} to 8 cm^{-1}. The barium atom number density was kept constant at $N_{Ba} = 1 \cdot 10^{12}$ cm^{-3} ($T \approx 850$ K). The variation of the barium number density from $5 \cdot 10^{11}$ cm^{-3} to $1.5 \cdot 10^{12}$ cm^{-3} at constant Ar pressure showed no changes in the diffusion distributions within error bars. Taking into account all experimental distributions curves, we have determined the values $A(^1D_2) = \alpha^2 D$. The diffusion coefficients were calculated according to (18). To our knowledge there are no D_0 data for Ba $^1D_2$ diffusion in Ar published in the literature. Because the diameters of barium in the metastable states considered are not very different, the diffusion coefficients of Ba ($^1D_2$) and Ba (^3D_J) should be of similar size. Therefore, we used a published Ba ^3D_J value [17] for the evaluation of $A(^1D_2)$. The calculated $A(^1D_2)$ data are plotted versus argon pressure in Fig. 15b. The least-square fit through the data is a straight line which intercepts the ordinate at $A_r(^1D_2) = 2.7 \cdot 10^3$ s^{-1}. This residual value $A_r(^1D_2)$ includes the spontaneous relaxation rate as well as possible depopulation rates by collisions with barium ground-state atoms. Thus, the total relaxation rate for Ba $^1D_2$ level can be written as:

$$A(^1D_2) = A_r(^1D_2) + N_{Ar}\sigma_{Ar}(^1D_2)v_{Ba-Ar}. \quad (28)$$

The depopulation cross section $\sigma_{Ar}(^1D_2)$ of the $^1D_2$ level due to collisions with argon was derived from the slope of the fitted straight line in Fig. 15b. The mean relative velocity $v_{Ba-Ar} = 7.35 \cdot 10^4$ cm s^{-1} was used which is an average value for the temperature range applied in the experiment. The following depopulation cross section was found:

$$\sigma_{Ar}(^1D_2) = 1.5 \cdot 10^{-17}\ \text{cm}^2. \quad (29)$$

The statistical accuracy of this cross section as well as of the $A_r(^1D_2)$ value is estimated to be about 30%.

Since the spontaneous relaxation rate for $^1D_2$ level is reported to be of the order of 10 s^{-1} [5], the value of $A_r(^1D_2)$ can be related to the depopulation by collisions between Ba $^1D_2$ and Ba $^1S_0$ atoms. According to our data we estimate the corresponding cross section to be $\sigma_{Ba}(^1D_2) = (55 \pm 30) \cdot 10^{-15}$ cm^2. Note that this value is of

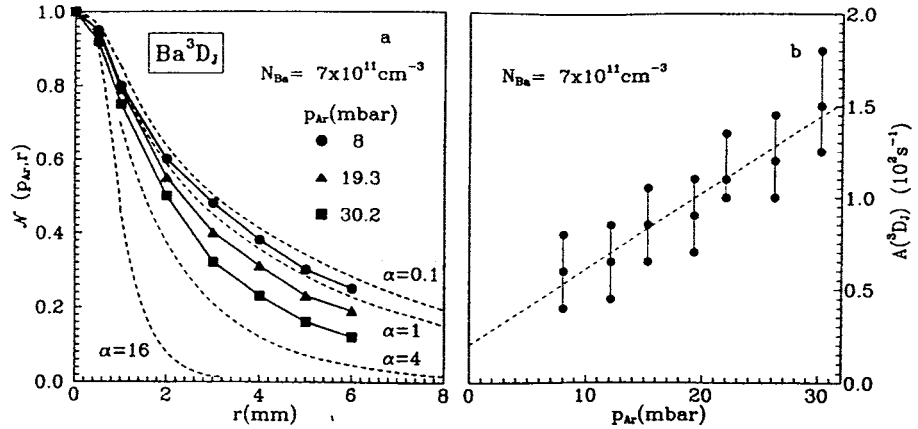

Fig. 16. **a** The measured and calculated distributions for Ba ^3D_J diffusion in argon. The measurements were performed at constant Ba ground state number density. **b** The relaxation rates of the ^3D_J level, deduced from the data in part **a** of this figure, plotted against argon pressure. For particular pressures the evaluation took into account the data at r = 3, 4, 5 cm

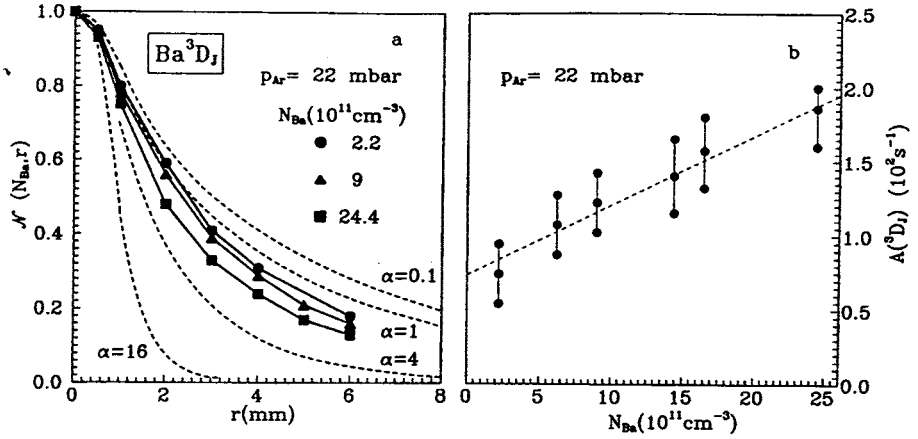

Fig. 17. **a** The measured and calculated distributions for Ba ^3D_J diffusion in argon. The measurements were done at constant Ar pressure but different Ba number densities. **b** The relaxation rates of the ^3D_J level deduced form the data in part **a** of this figure plotted against barium number density. For particular Ba number densities the evaluation took into account the data at r = 3, 4, 5 cm

the same order of magnitude as the cross section for $^1D_2 \rightarrow {}^3D_J$ transition induced by Ba $^1D_2$ collisions with Ba ground state atoms [9, 10].

4.7 Relaxation of the barium ^3D_J atoms

The distribution curves for the diffusion of Ba ^3D_J atoms in Ar were measured in the pressure range between 8 and 30 mbar. Ba ^3D_J metastables can be produced by transitions from the $^3P_1^0$ and $^1D_2$ levels. Here, the choice of a rectangular source function is questionable for the theoretical simulation. However, a rectangular shaped source function is justified for the $^3P_1^0 \rightarrow {}^3D_J$ population channel in the same way as it was for Ba $^1D_2$. Nevertheless, under the present experimental conditions the same is justified for the $^1D_2 \rightarrow {}^3D_J$ collisional population, since the Ba $^1D_2$ metastables are mostly confined within the laser beam volume for the applied Ar pressure. This was proved by measurements of the distribution of Ba $^1D_2$, but it can be also taken from the results given above. For instance, the relaxation rate $A(^1D_2)$ is about $1.5 \cdot 10^5$ s^{-1} at Ar pressure of 15 mbar. With the corresponding diffusion coefficient $D = 30$ cm^2 s^{-1} the parameter α is about 70 cm^{-1}. It means that the distribution of Ba $^1D_2$ is nearly rectangularly shaped.

The results obtained for the Ba ^3D_J distributions at different argon pressures are shown in Fig. 16a. Analogously to the case of $^1D_2$ atoms, the calculated values of the Ba ^3D_J relaxation rates exhibit a linear dependence on the buffer gas pressure (Fig. 16b). Compared with $A(^1D_2)$, the obtained $A(^3D_J)$ values are more than two orders of magnitude smaller. Furthermore, the distributions of ^3D_J metastable atoms show, differently to those in the $^1D_2$ state, a clear dependence on the Ba ground-state atom number density (Fig. 17a). The argon pressure was kept constant (22 mbar) while the temperature was varied between 770 and 900 K, yielding Ba number densities in the range $2.2 \cdot 10^{11} - 2.4 \cdot 10^{12}$ cm^{-3}. The evaluated relaxation rates $A(^3D_J)$ are linearly dependent on the barium number density (Fig. 17b). Therefore, the total relaxation rate $A(^3D_J)$ can be expressed in the following way:

$$A(^3D_J) = A_r(^3D_J) + N_{Ba}\sigma_{Ba}(^3D_J)v_{Ba-Ba} + N_{Ar}\sigma_{Ar}(^3D_J)v_{Ba-Ar}. \quad (30)$$

With the data shown in Fig. 16b we have obtained the following cross section for the collisional depopulation of the ^3D_J level by argon:

$$\sigma_{Ar}(^3D_J) = 7 \cdot 10^{-21}\ \text{cm}^2, \quad (31)$$

while the data in Fig. 17b yielded the collisional depopulation cross section of ^3D_J atoms by barium ground-state atoms:

$$\sigma_{Ba}(^3D_J) = 1 \cdot 10^{-15}\ \text{cm}^2. \quad (32)$$

The statistical accuracy of the given cross sections is about 20%.

The residual relaxation rate $A_r(^3D_J)$ was calculated taking into account σ_{Ar}, σ_{Ba} and the data displayed in Fig. 16 as well as in Fig. 17. The obtained value is very small compared with the error bar. It is of the order of magnitude 0 to 20 s^{-1} which corroborates the small theoretical lifetime value of 60 s [5].

5 Discussion

5.1 Collisional depopulation of the $^3P_1^0$ state

As pointed out in Sect. 4.3, the whole deactivation of the $^3P_1^0$ level is related to direct collisional production of $^1D_2$ and ^3D_J atoms. This conclusion is in agreement with recent timeresolved measurements in barium-noble gas mixtures [11]. Moreover, as can be seen in Table 1, our data of the $^3P_1^0$ depopulation cross sections by He, Ar and Xe are in fair agreement with the values measured by [11].

Considering the branching ratio for $^3P_1^0 \rightarrow {}^1D_2, {}^3D_J$ collisional transitions, we have combined the results presented in Sect. 4.4, 4.6 and 4.7. Since only for Ar was a complete set of data obtained, this consideration is limited to Ar for which, in contrast to the other noble gases used in the present experiment, the mixing between the $^1D_2$ and ^3D_J states is extremely weak. In a first step, we suppose that both $^1D_2$ and ^3D_J levels are populated collisionally from the $^3P_1^0$ level with the rates R_1 and R_3, respectively. In addition, the ^3D_J level is radiatively populated with the rate $A_{23} = 5.3 \cdot 10^5 s^{-1}$ [13], and the steady-state rate equations for these levels can be written as:

$$N(^3P_1^0)R_1 - N_t(^1D_2)A(^1D_2) = 0, \tag{33}$$

$$N(^3P_1^0)(R_3 + A_{23}) - N_t(^3D_J)A(^3D_J) = 0. \tag{34}$$

Here, the number densities $N_t(^1D_2)$ and $N_t(^3D_J)$, which will be called total number densities, are related to the total number of singlet and triplet atoms created in the excitation volume per unit time, respectively.

Table 1. Depopulation cross sections of excited barium levels by noble gases. The values of the cross sections are given in 10^{-16} cm^2

	$\sigma(^3P_1^0)$	$\sigma(^1D_2 \rightarrow {}^3D_J)$	$\sigma(^1D_2 \rightarrow {}^3D_3)$
He	5.5 ± 1.5[a]		
	3.51 ± 0.04[b]		5.27 ± 0.5[b]
		0.1 ± 0.06[c]	
		0.12 ± 0.03[d]	
Ar	4.6 ± 1.5[a]	0.015 ± 0.010[a]	
	5.35 ± 0.05[b]		0.037 ± 0.005[b]
		0.5 ± 0.3[c]	
Xe	1.7 ± 0.5[a]		
	1.06 ± 0.02[b]		0.62 ± 0.04[b]

[a] Present results, column one: $T = 760$ K; column two: $T = 860$ K
[b] [11], column one: $T = 775$ K; column three: $T = 880$ K
[c] [9], $T = 1100$ K
[d] [10], $T = 1000$ K

These number densities include the diffusion out of the excitation zone, and their ratio χ can be described by

$$\chi = \frac{N_t(^1D_2)}{N_t(^3D_1)} = \frac{N(^1D_2)}{N(^3D_1)} \frac{\int r\aleph_1(r)\,dr}{\int r\aleph_3(r)\,dr}. \tag{35}$$

Here, $\aleph_1(r)$ and $\aleph_3(r)$ are the normalized (as explained in Sect. 4.4) radial distributions of singlet and triplet atoms, respectively, while $N(^1D_2)/N(^3D_J)$ is the singlet to triplet number density ratio on the axis of the exciting zone, as given in Sect. 4.2. The $N(^1D_2)/N(^3D_J)$ decreases from 0.055 to about 0.033 if the Ar pressure is varied between 20 and 30 mbar. Including this information, we deduced the value of χ from the data presented in Sect. 4.6 and 4.7. The ratio $\int r\aleph_1(r)dr/\int r\aleph_3(r)dr$, not shown graphically, increases from 0.05 to 0.07 with pressure, and the product of $\int r\aleph_1(r)dr/\int r\aleph_3(r)dr$ and $N(^1D_2)/N(^3D_J)$ giving χ, decreases slowly from 0.0030 to 0.0025. By combination of (33), (34) and (35) one obtains:

$$\frac{R_1}{R_3 + A_{23}} = \varphi, \tag{36}$$

where $\varphi = \chi A(^1D_2)/A(^3D_J)$. Using the data for $A(^1D_2)$ and $A(^3D_J)$. given in Sect. 4.6 and 4.7, respectively, we found values of φ of about 6. From this follows immediately that $R_1 \gg R_3$. Using (36) with $R = \sigma_{Ar}(^3P_1^0) \cdot N_{Ar} \cdot v_{Ba-Ar} = R_1 + R_3$, we evaluated the values for the cross sections σ_1 and σ_3 (Fig. 18). For the collisional transition $^3P_1 \rightarrow {}^1D_2$, the cross section is $\sigma_1 \approx \sigma_{Ar}(^3P_1^0)$. Unfortunately, this method is inaccurate for the evaluation of the σ_3 collisional cross section for the $^3P_1^0 \rightarrow {}^3D_J$ transitions. The evaluation gives results scattered within the error bar of $\pm 1 \cdot 10^{-16}$ cm^2 around the zero mean value. Therefore, the only conclusion which can be given is $\sigma_3 \ll \sigma_{Ar}(^3P_1^0)$. As a result, we conclude that the main depopulation channel for $^3P_1^0$ is given by $^3P_1^0 \rightarrow {}^1D_2$ collisional transitions at our experimental conditions.

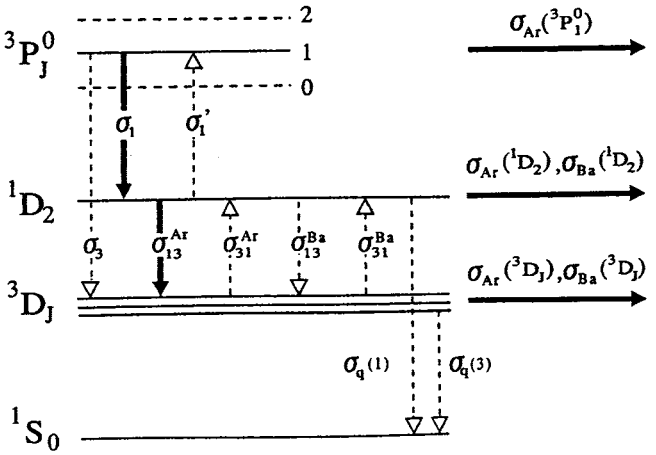

Fig. 18. The lowest lying barium states with relevant collisional transitions. *Bold arrows*, the transitions for which the cross sections have been measured in this work. *Dashed arrows*, other relevant collisional transitions. Note, *horizontal bold arrows* are related to the total depopulation by collisions with argon or barium ground state atoms

The same conclusion has been drawn from the time-resolved measurements by [11]. For this particular relaxation process, it is obvious that time-resolved measurements have the advantage to provide a clearer insight. In [11] it was found that for all noble gases (He, Ne, Ar, Kr and Xe), the dominant depopulation process for $^3P_1^0$ level is the transfer to $^1D_2$ and subsequent $^1D_2$ transfer to the $^3D_3$. Furthermore, it was observed that the $^3D_1$ and $^3D_2$ triplet sublevels are populated by collisional mixing with $^3D_3$. No transfer between $^3P_1^0$ and ^3D_J was detected.

5.2 Collisional population of the ^3D_J state

From the findings above it can be concluded that for argon buffer gas the only collisional population channel for ^3D_J level is a weak $^1D_2 \rightarrow {}^3D_J$ process. Consequently, the steady-state rate equation for the ^3D_J level is given, instead of (34), by:

$$N(^3P_1^0)A_{23} + N_t(^1D_2)R_{13} - N_t(^3D_J)A(^3D_J) = 0. \quad (37)$$

Here, R_{13} is the rate for $^1D_2 \rightarrow {}^3D_J$ collisional transitions, which, according to (33), (35) and (37), is given by

$$R_{13} = \frac{A(^3D_J)}{\chi} - A_{23}\frac{A(^1D_2)}{R_1}. \quad (38)$$

The corresponding cross section σ_{13}^{Ar} obtained in this way is

$$\sigma_{13}^{Ar} = 1.5 \cdot 10^{-18}\ \text{cm}^2. \quad (39)$$

The accuracy of this cross section is estimated to be about $\pm$ 70%. Note, that this value represents the maximum value possible, since σ_3 is supposed to be zero.

The cross sections for $^1D_2 \rightarrow {}^3D_J$ collisional transfer induced by He, Ar and Xe reported by [11], as well as earlier results obtained for the same process in He and Ar [9, 10], are given in Table 1. Our value for Ar is about three times smaller than the result obtained by [11], and about forty times smaller than the datum of [9]. The qualitative results for He and Xe, presented in Sect. 4.4, are in accordance with the data obtained by [11]. Actually, we have observed the reverse transfer process $^3D_J \rightarrow {}^1D_2$, which is very weak in Ar, stronger in Xe and very strong in He. Note, that these mutual relationships are in agreement with the data obtained by [11], but disagree with what was reported in [9].

5.3 Collisional depopulation of the ^3D_J state

According to the principle of detailed balancing, the ratio of the cross sections σ_{13} and σ_{31} for the processes $^1D_2 \rightarrow {}^3D_J$ and $^3D_J \rightarrow {}^1D_2$, respectively, should be 110:1, if the average temperature in our experiment is taken into account. Using the value for σ_{13}^{Ar} given by (39), one obtains $\sigma_{31}^{Ar} = (1.2 \pm 0.7) \cdot 10^{-20}\ \text{cm}^2$. This is very close to our measured value for the total depopulation cross section $\sigma_{Ar}(^3D_J) = (7 \pm 1.5) \cdot 10^{-21}\ \text{cm}^2$, given by (31). The comparison implies that the main process responsible for collisional depopulation of Ba ^3D_J by argon is:

$$\text{Ba}(^3D_J) + \text{Ar} \xrightarrow[\sigma_{Ar}(^3D_J)]{} \text{Ba}(^1D_2) + \text{Ar}. \quad (40)$$

We will attempt to describe the deactivation of ^3D_J by collisions with barium ground state atoms. The measured cross section $\sigma_{Ba}(^3D_J)$ can be related to the quenching process $\text{Ba}(^3D_J) + \text{Ba}(^1S_0) \xrightarrow[\sigma_q(3)]{} 2\text{Ba}(^1S_0)$ and to the intermultiplet mixing process $\text{Ba}(^3D_J) + \text{Ba}(^1S_0) \xrightarrow[\sigma_{31}^{Ba}]{} \text{Ba}(^1D_2) + \text{Ba}(^1S_0)$. If we attribute the measured $\sigma_{Ba}(^3D_J)$ value solely to the intermultiplet mixing, the principle of detailed balancing predicts $\sigma_{13}^{Ba} = (1 \pm 0.5) \cdot 10^{-13}\ \text{cm}^2$, where $\sigma_{31}^{Ba} = \sigma_{Ba}(^3D_J)$. This cross section coincides with the data reported in [9, 10] for $^1D_2 \rightarrow {}^3D_J$ transfer by collisions with barium ground state atoms, and also with our estimated value for $\sigma_{Ba}(^1D_2)$ (Sect. 4.6). The consideration above implies that quenching by Ba ($^1S_0$) atoms is not the main process responsible for the deactivation of $^1D_2$ or ^3D_J states. The deactivation of these states due to collisions with barium ground state atoms can be explained by their mixing. Note, that in this case the rate R_{13} in (38) should include the contribution which corresponds to the $^1D_2 \rightarrow {}^3D_J$ transition induced by collisions with Ba ($^1S_0$) atoms. Therefore, the reported value for σ_{13}^{Ar} should actually be about 30% lower, thus yielding even better agreement between the σ_{31}^{Ar} value obtained from the principle of detailed balancing and measured total depopulation cross section $\sigma_{Ar}(^3D_J)$.

Our $\sigma_{Ba}(^3D_J)$ value is about ten times smaller than that reported previously by [18]. In the paper [18] a cross section of about $1.3 \cdot 10^{-14}\ \text{cm}^2$ was deduced from the decay of the ^3D_J state at $T = 730$ K and about 60 mbar He, assuming that collisions with He are negligible. We believe that under the experimental conditions of [18], this particular process is not negligible.

Moreover, as it has been recently confirmed by the measurements of [11], the collisions with He are dominant at the experimental conditions chosen by [18].

5.4 Collisional depopulation of the $^1D_2$ state

The total cross section for the depopulation of $^1D_2$ state by Ar is related to the processes $^1D_2 \rightarrow {}^3D_J$ and $^1D_2 \rightarrow {}^3P_1^0$, i.e., $\sigma_{Ar}(^1D_2) = \sigma_{13}^{Ar} + \sigma_1'$ (see Fig. 18). Since σ_{13}^{Ar} is one order of magnitude lower than $\sigma_{Ar}(^1D_2)$, the main channel for the deactivation of the $^1D_2$ state is transfer to $^3P_1^0$. This means that, according to the principle of detailed balance, $\sigma_{Ar}(^3P_1^0)$ and $\sigma_1' \cong \sigma_{Ar}(^1D_2)$ should have the ratio 1:18. Indeed, using (26) we obtain $\sigma_1' = (0.25 \pm 0.8) \cdot 10^{-16}\ \text{cm}^2$ which is, within the limits of uncertainty, in agreement with the measured value for $\sigma_{Ar}(^1D_2) = (1.5 \pm 0.5) \cdot 10^{-17}\ \text{cm}^2$. Therefore, we conclude that the process

$$\text{Ba}(^1D_2) + \text{Ar} \xrightarrow[\sigma_1']{} \text{Ba}(^3P_1^0) + \text{Ar}, \quad (41)$$

is the main process for collisional deactivation of the $^1D_2$ state by argon. The same conclusion has been made qualitatively in [11].

6 Conclusion

The cross sections for the depopulation of the Ba $^3P_1^0$ state, induced by collisions with He, Ar and Xe, have been measured, and the values of $\sigma_{He}(^3P_1^0) = 5.5 \cdot 10^{-16}$ cm^2, $\sigma_{Ar}(^3P_1^0) = 4.6 \cdot 10^{-16}$ cm^2 and $\sigma_{Xe}(^3P_1^0) = 1.7 \cdot 10^{-16}$ cm^2 have been obtained. In the case of Ar we have found that the collisional depopulation of the $^3P_1^0$ level is related exclusively to the transition of the $^1D_2$ metastable state. Assuming the ^3D_J metastable state to be populated collisionally by $^1D_2 \rightarrow {}^3D_J$ transfer only, we have deduced the upper limit for the corresponding cross section $\sigma_{13}^{Ar} = 1.5 \cdot 10^{-18}$ cm^2. Furthermore, the steady-state diffusion distributions of the Ba $^1D_2$ and Ba ^3D_J metastables have been measured and compared with the theoretical curves. With the known diffusion coefficient for barium in argon, collisional relaxation rates of the $^1D_2$ and ^3D_J levels were found. The relaxation rates were measured in dependence on argon and barium pressure. From these data the total cross sections for the depopulation of $^1D_2$ and ^3D_J levels by collisions with Ar as well as with Ba ground state atoms were determined. The experimental values are: $\sigma_{Ar}(^1D_2) = 1.5 \cdot 10^{-17}$ cm^2, $\sigma_{Ba}(^1D_2) \cong 1 \cdot 10^{-13}$ cm^2, $\sigma_{Ar}(^3D_J) = 7 \cdot 10^{-21}$ cm^2, and $\sigma_{Ba}(^3D_J) = 1 \cdot 10^{-15}$ cm^2.

Using the principle of detailed balancing, we have found that the main part of the collisional depopulation of the $^1D_2$ state by Ar is related to back transfer to the $^3P_1^0$ state. Applying the same principle we have also concluded that the deactivation of the ^3D_J metastable state is due to back transfer to the $^1D_2$ state. In the case of argon as a perturber, the experimental data reported in this work were sufficient to make such conclusions. In the case of collisional depopulation of the $^1D_2$ and ^3D_J levels by barium ground state atoms, the values obtained by taking into account the principle of the detailed balancing, were compared with results reported in literature. This comparison gave the hint that collisional deactivation of both metastable levels by barium ground state atoms can be attributed to their mutual collisional mixing.

We acknowledge gratefully financial support by the Deutsche Forschungsgemeinschaft (project no. Ni 185/17) and by the Ministry of Science (Republic of Croatia).

References

1. Vadla, C., Niemax, K., Horvatic, V.: to be published
2. Obrebski, A., Hergenröder, R., Niemax, K.: Z. Phys. D14, 289 (1989)
3. Obrebski, A., Lawrenz, J., Niemax, K.: Spectrochim. Acta 45B, 15 (1990)
4. Klimovskii, I.I., Minaev, P.V., Morozov, A.V.: Opt. Spektrosk. 50, 847 (1981)
5. Migdalek, J., Baylis, W.E.: Phys. Rev. A42, 6897 (1990)
6. Ehrlacher, E., Huennekens, J.: Phys. Rev. A46, 2642 (1992)
7. Kallenbach, A., Günther, M., Künnemeyer, R., Kock, M.: J. Phys. B19 , 2645 (1986)
8. Breckenridge, W.H., Merrow, C.N.: J. Chem. Phys. 88, 2329 (1988)
9. Kallenbach, A., Kock, M.: J. Phys. B22, 1705 (1989)
10. Bowen, J.L., Thorne, A.P.: J. Phys. B18, 35 (1985)
11. Brust, J., Gallagher, A.C.: Phys. Rev. A (submitted)
12. Mitchell, A.G.C., Zemansky, M.W.: Resonance radiation and excited atoms. Cambridge: Cambridge University Press 1971
13. Bauschlicher, C.W., Jaffe, R.L., Langhoff, F.G., Mascarello, F.G., Partrige, H.: J. Phys. B18, 2147 (1985)
14. Niggli, S., Huber, M.C.E.: Phys. Rev. A35, 2907 (1987)
15. Ehrlacher, E., Huennekens, J.: Phys. Rev. A47, 3097 (1993)
16. Nesmeyanov, A.N.: Vapor pressure of the elements. New York: Academic Press 1963
17. Walker, T.G., Bonin, K., Happer, W.: J. Chem. Phys. 87, 660 (1987)
18. Whitkop, P.G., Wiesenfeld, J.R.: J. Chem. Phys. 72, 1297 (1980)